Physica D 238 (2009) 1490–1495

Contents lists available at ScienceDirect

Physica D

journal homepage: www.elsevier.com/locate/physd

Non-quantum liquefaction of coherent gases

David Novoa *, Humberto Michinel, Daniele Tommasini, María I. Rodas-Verde

Departamento de Física Aplicada, Facultade de Ciencias de Ourense, Universidade de Vigo, As Lagoas s/n, Ourense, ES-32004, Spain

ARTICLE INFO

Article history:
Available online 10 February 2009

PACS:
03.75.Lm
42.65.Jx
42.65.Tg

Keywords:
Phase transition
Liquefaction
solitons
Filamentation
Cold atoms

ABSTRACT

We show that a gas-to-liquid phase transition at zero temperature may occur in a coherent gas of bosons in the presence of competing nonlinear effects. This situation can take place in atomic systems like Bose–Einstein condensates in alkali gases with two-body and three-body interactions of opposite signs, as well as in laser beams which propagate through optical media with Kerr (focusing) and higher order (defocusing) nonlinear responses. The liquefaction process takes place in the absence of any quantum effect and can be formulated in the framework of a mean field theory, in terms of the minimization of a thermodynamic potential. We study from a thermodynamic point of view all the stationary solutions of the cubic–quintic nonlinear Schrödinger equation which describes our system. We show that solitonic localized solutions connect the gaseous and liquid phases. Furthermore, we also perform a numerical simulation in the presence of linear gain and three-body recombination where a rich dynamics, including the emergence of self-organization behavior, is found.

1. Introduction

Paraxial propagation of linearly polarized laser beams through transparent optical media with intensity dependent refractive indexes is mathematically equivalent to the free evolution of the wavefunction order parameter used in the mean field description of a two-dimensional gas of N interacting atoms in a Bose–Einstein Condensate (BEC) at temperature $T = 0$ K [1]. The two systems can be modeled by identical nonlinear Schrödinger equations [2]. For photons in the laser beam, the $\chi^{(n)}$ component of the nonlinear optical susceptibility plays the same role as n-body interactions between atoms in the cloud, and the propagation constant can be identified with a chemical potential for the light distribution. As all the photons in a coherent wave are equal, the laser beam can be treated on an equal footing with any system of N identical interacting bosons at zero temperature [3].

The previous point of view, which takes into account the equivalence between laser beams and BECs of ultracold atoms, has led to an interesting suggestion made by Chiao [4], who recently proposed verifying the superfluidity of coherent light, in analogy with degenerate quantum atomic gases. More recently, similar concepts have been successfully used to analyze condensation phenomena of nonlinear waves [5] and quantum phase transitions of photons in periodic lattices [6].

In Chiao's model the key point of the analysis is *"same equations, same predictions"* and therefore photons from a monochromatic laser source are considered as an ideal bosonic gas at zero temperature in which continuous phase transitions (CPT) can take place due to long range quantum fluctuations around the ground state [7]. These critical phenomena are thus called *quantum* phase transitions (QPT) [8] to distinguish them from the standard phase changes which are well-known in classical thermodynamics.

As we will show in this work, CPT may occur in any *classical* system at zero temperature without long range quantum correlations being involved, if opposite nonlinear interactions are present. In the case of Chiao's "superfluid light" the phase transition is produced by the effect of a defocusing intensity dependent refractive index [9] and thus a waveguide is used to avoid spreading of the beam (in the same way as magneto-optical traps are employed to hold atomic BECs). In the previous case there is no trace of the presence of a liquid state [10,11] as there are no surface tension effects [12]. Moreover, in Chiao's model, the interactions between particles are repulsive and they cannot drive a gas–liquid transition.

Thus, in this work we will follow the same lines of thought to suggest the possibility of obtaining a gas-to-liquid phase transition in a classical gas at $T = 0$ K described in a mean field theory by the so-called *cubic–quintic* (CQ) model with competing nonlinearities. Several pioneering works have highlighted the interesting properties of this CQ model [13,14]. Cavitation, superfluidity and coalescence have been investigated [15–17] in the context of liquid He, where the model is a simple approach if nonlocal interactions are not taken into account. Stable optical vortex solitons and the existence of top-flat states have been also reported in optical materials with CQ optical susceptibility [18,19]. The surface tension properties that appear in this system [20] have been considered as a trace of a "liquid state of light" [10].

* Corresponding author. Tel.: +34 988387242; fax: +34 988387227.
E-mail address: dnovoa@uvigo.es (D. Novoa).

0167-2789/$ – see front matter © 2009 Elsevier B.V. All rights reserved.
doi:10.1016/j.physd.2009.02.002

On the other hand, recent experiments concerning filamentation of high-power laser pulses in CS_2 have shown that CQ nonlinearity is achievable in this material [21]. It has also been suggested that atomic coherence may be used to induce a giant CQ-like refractive index of Rb gas [11]. Thus, the practical realization of the first "liquid of light" state as an example of non-quantum liquefaction at zero temperature is close.

2. Mathematical analysis

The cubic–quintic model describes a coherent bosonic system of N particles with two-body and three-body interactions. The mathematical formulation of the mean field theory yields a generalized nonlinear Schrödinger (NLS, also called Gross–Pitaevskii) equation of the form

$$\mathrm{i}\frac{\partial\Psi}{\partial\eta}+\frac{1}{2}\nabla_\perp^2\Psi+\gamma|\Psi|^2\Psi-\delta|\Psi|^4\Psi=0. \tag{1}$$

If the system modeled by the previous equation is a photon gas, the above NLS describes paraxial propagation of a continuous linearly polarized laser beam of wavelength λ in a nonlinear medium with a refractive index depending on the intensity I in the form $n = n_0 + n_2 I - n_4 I^2$ and the adimensional variables are: η, the propagation distance multiplied by $2\pi/\lambda$; $|\Psi|^2$, the beam irradiance multiplied by the Kerr coefficient $n_2 = \gamma$; $n_4 = \delta$, an adimensional parameter indicating the strength of the quintic nonlinear optical susceptibility; and $\nabla_\perp^2 = \partial^2/\partial x^2 + \partial^2/\partial y^2$, the transverse Laplacian operator, where x and y are the transverse spatial dimensions multiplied by $2\pi\sqrt{2n_0}/\lambda$.

In the case of a two-dimensional atomic BEC tightly trapped along one axis by a parabolic potential of frequency $\nu_\perp$ and thickness $r_\perp = \sqrt{\hbar/m\nu_\perp}$, the adimensional variables correspond to: η, the time in units of $\nu_\perp^{-1}$; $|\Psi|^2$, the atomic density multiplied by the two-body coefficient γ; δ, an adimensional parameter indicating the strength of the three-body interactions; and $\nabla_\perp^2 = \partial^2/\partial x^2 + \partial^2/\partial y^2$, the transverse Laplacian operator, where x and y are the transverse spatial dimensions divided by $r_\perp$.

Recent experiments for beam propagation in CS_2 [21] at $\lambda = 800$ nm yield the following values for the above parameters in the case of laser beams: $n_0 = 1.6$, $n_2 = 3\cdot10^{-15}$ cm^2/W and $n_4 = 2\cdot10^{-27}$cm^4/W^2. Other materials like air [22] or chalcogenide glasses [23] seem to display the CQ behavior usually accompanied by ionization and nonlinear losses. There has also been pointed out the possibility of engineering this type of optical response by quantum techniques which allow one to access this nonlinear regime with milliwatt ultrastabilized lasers [11]. For atomic BEC systems it has been proposed that a combination of two-body (attractive) and three-body (repulsive) elastic interactions can yield liquid *boselets* [24]. However, three-body scattering in BECs has inelastic contributions and yields highly nonlinear losses. This means that in the most general case the coefficient δ in Eq. (1) may be complex for laser systems as well as for atomic gases.

The above CQ NLSE admits soliton-like solutions of finite size [13] of the form $\Psi_A(x,y,\eta) = A(x,y)\mathrm{e}^{-\mathrm{i}\mu\eta}$, μ being the propagation constant in the case of light and the chemical potential for atomic BECs. These solitons can only be calculated numerically. They coexist with plane wave solutions of constant amplitude $\Psi_A(x,y,\eta) = A\mathrm{e}^{-\mathrm{i}\mu\eta}$, in which case, by substituting in Eq. (1), we get the analytical relation

$$\mu=\delta|A|^4-\gamma|A|^2. \tag{2}$$

In Fig. 1 we have plotted the maximum value of $\gamma|\Psi|^2$ versus μ for different kinds of stationary solutions of Eq. (1). The continuous and dotted lines correspond respectively to stable and modulationally unstable plane waves [25], whereas the dashed line

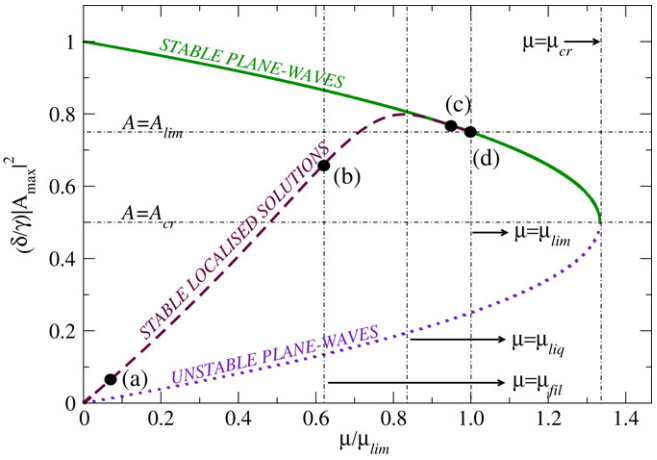

Fig. 1. [Color online] Maximum squared amplitude of different kinds of stationary solutions of Eq. (1). The continuous and dotted curves correspond to plane waves. The dashed line represents numerically calculated localized eigenstates. The continuous and dashed curves join at $(\delta/\gamma)|A_{\max}|^2 = 0.75$, $|\mu| = |\mu_{\mathrm{eq}}|$. Horizontal lines indicate the critical values $(\delta/\gamma)|A_{\max}|^2 = 0.5$ and $(\delta/\gamma)|A_{\max}|^2 = 0.75$. Labeled points correspond to solitons that are considered as special examples in the text.

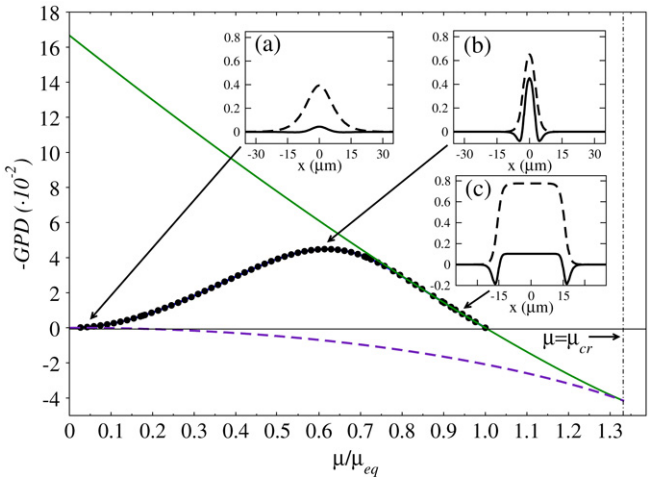

Fig. 2. [Color online] Plots of minus the grand potential density ($-GPD = -\frac{\partial\Omega}{\partial\delta}$) for the plane wave solution branches of Fig. 1 (green solid, stable; purple dashed, unstable) and its value at the center ($x = 0$) of the eigenstates (thick dotted line) corresponding to different points in the dashed line of Fig. 1 (assuming $\gamma = \delta = 1$). Insets: profiles of the eigenstates (dashed) and $-GPD$ distribution (solid). The x axis indicates the transverse size of the numerically calculated distributions of different eigenstates of Eq. (1). We have multiplied $\gamma|\Psi|^2$ and p by 10 and 100 respectively in (a) and p by 10 elsewhere.

stands for numerically calculated localized eigenstates [26]. As is known [18], the shapes of the solitons (see the dashed profiles in Fig. 2) vary from quasi-gaussian for low powers to almost square profiles for beam amplitudes close to a limiting value of $\mu = \mu_{\mathrm{lim}} = -0.1875\gamma^2/\delta$ [18,26]. At this point the size of the solutions tends to infinity whereas the amplitude of the beam stabilizes at $|A_{\max}|^2 = |A_{\mathrm{lim}}|^2 = 0.75\gamma/\delta$.

For convenience, in Fig. 1 we have scaled the horizontal, μ axis, in units of μ_{lim}. We also define $|\mu_{\mathrm{liq}}|$ as the value of μ for which the peak amplitude of the localized solutions in Fig. 1 is maximum. We see in Fig. 1 that the localized solution and stable plane wave branches seem to merge there. Moreover, all the solitons having $|\mu| > |\mu_{\mathrm{liq}}|$ turn out to have a top-flat shape, that has been shown to behave like a liquid [10]. We leave for the next section the definition of the other critical value $\mu = \mu_{\mathrm{fil}}$, which arises from the thermodynamical analysis of the eigenstates.

3. Thermodynamic model

The appropriate tool for studying the equilibrium condition as a function of the number of particles $N = \int |\Psi|^2 \mathrm{d}x\mathrm{d}y$ is Landau's grand potential

$$\Omega = H - \mu N = \int \mathrm{d}x\mathrm{d}y \left[\frac{1}{2}|\nabla_\perp \Psi|^2 - \frac{\gamma}{2}|\Psi|^4 + \frac{\delta}{3}|\Psi|^6 - \mu|\Psi|^2\right], \tag{3}$$

where the Lagrange multiplier μ is the chemical potential for a BEC. By requiring that Eq. (1) corresponds to $\frac{\delta\Omega}{\delta\psi^*} = 0$ for the stationary solution, we have that μ has to be equal to the propagation constant that we have introduced above.

In two dimensions, it is then natural to define the partial derivative $(\partial\Omega/\partial\mathcal{A})_{\mu,T}$ of the grand potential Ω with respect to the area $\mathcal{A}$ at constant chemical potential μ and temperature T. This yields the following grand potential density (*GPD*):

$$GPD = (\partial\Omega/\partial\mathcal{A})_{\mu,T} = +\frac{1}{2}|\nabla_\perp \Psi|^2 - \frac{\gamma}{2}|\Psi|^4 + \frac{\delta}{3}|\Psi|^6 - \mu|\Psi|^2. \tag{4}$$

In the region of space where the gradient term can be neglected, this definition reproduces the approximate result that has been obtained in Ref. [15] using Madelung transformations [27] in the particular case of plane wave or top-flat solutions,

$$(\partial\Omega/\partial\mathcal{A})_{\mu,T} = -\frac{2\delta}{3}|A|^6 + \frac{\gamma}{2}|A|^4. \tag{5}$$

Note that the latter equation also uses Eq. (2), which is only correct for the plane waves and for the top-flat solutions far enough from the boundary of the liquid drop. On the other hand, our new result Eq. (4) is more general, since it takes into account the gradient term, and can also be used to describe the behavior near the border of the top-flat solitons. Moreover, it can also be applied to the low power, quasi-gaussian solitons, for which the gradient term is not negligible, provided that the correct numerical value of μ is used. The numerical result for the computation of *GPD* in the whole space for both the top-flat and for the quasi-gaussian solitons is given in Fig. 2, which will be discussed below.

Although all the solutions of Eq. (1) correspond to $\frac{\delta\Omega}{\delta\psi^*} = 0$, we find two or three different kinds of solutions, depending on the value of μ, as shown in Fig. 1. From Fig. 2, we see that the lower-branch plane waves, corresponding to the gaseous phase, have positive density of Ω, while the higher-branch plane waves, corresponding to the liquid phase, have negative density of Ω. This thermodynamic argument shows that the gaseous phase is metastable. In fact, the analysis of linear stability that has been performed in the literature [25,16] using non-zero wavevector perturbations, together with our numerical simulations, confirms that the gaseous phase is indeed modulationally unstable.

From Fig. 2, we also see that there are two configurations having $\partial\Omega/\partial\mathcal{A} = 0$, namely, the trivial case $|A| = 0$ and a uniform phase, with $\mu_{\mathrm{lim}} = -\frac{3\gamma^2}{16\delta}$ and $|A_{\mathrm{lim}}|^2 = 0.75\gamma/\delta$. In the language of field theory, these solutions are the two possible "vacuum" states of the system. As can be seen in Fig. 1 the two vacua can be "connected" by the soliton solutions of the dashed line in Fig. 1. It is interesting to note that the non-zero vacuum solution implies a spontaneous symmetry breaking of the global phase symmetry, which is preserved in the case with $|A| = 0$.

Let us now discuss in more detail our results for the *GPD*, which is plotted in Fig. 2 as a function of μ/μ_{lim}, for the same branches of solutions as were defined in Fig. 1. Very remarkable is the fact that the value of $-GPD$ for the stable branch is higher than that of the unstable branch. This implies that free energy density of the stable plane waves is smaller than the free energy of the modulationally unstable solutions branch. In Fig. 2 we also plot the curve of the central values of $-GPD$ for the eigenstates, as a function of μ/μ_{lim}. As can be seen from the graph, the curve corresponding to the eigenstates is bounded by the two curves of the plane wave branches, so the existence domain of the filament phase is limited by them. In the insets of Fig. 2, we show the shape profiles of the eigenstates (dashed line) superposed with their effective $-GPD$ profiles (solid lines), which have been conveniently rescaled to fit in the graph. As can be appreciated in inset (a), solitons with $|\mu| \ll |\mu_{\mathrm{lim}}|$ have smooth distributions with a central maximum located at the centroid of the soliton and two negative-valued minima. As the value of $|\mu|$ increases, the soliton profiles and their corresponding shapes of $-GPD$ narrow, reaching a minimum width at $\mu/\mu_{\mathrm{lim}} = 0.5$, which corresponds to a filament soliton solution with the same peak amplitude as the "critical" plane wave with $|A| = |A_{cr}|$. This plane wave marks the border between stable and modulationally unstable plane waves [15]. When the chemical potential reaches the value $|\mu| = |\mu_{\mathrm{fil}}|$ (see inset (b)), the absolute maximum of $-GPD$ for eigenstates is obtained, i.e., this filament has the minimum of $\mathrm{d}\Omega/\mathrm{d}\mathcal{A}$ at its centroid. For $|\mu_{\mathrm{liq}}| < |\mu| < |\mu_{\mathrm{lim}}|$, the minimum of the Landau's grand potential density is located in a flat region (see inset (c)), tending to zero as $|\mu|$ approaches the critical value $|\mu_{\mathrm{lim}}|$, point (d) in Fig. 1, over which no localized solutions exist [18].

In particular, the insets in Fig. 2 show a significant, qualitative difference between the distributions of the low-power quasi-gaussian solutions and that of the high-power top-flat solutions of Eq. (1). This can be considered as a new, further proof of the existence of two phases: the liquid and the gaseous.

4. Condensation in the presence of linear gain and nonlinear losses

In this section, we will provide a set of numerical simulations showing the condensation process, i.e., the phase transition from the gaseous phase to a homogeneous coherent "liquid" plane wave solution corresponding to the upper branch in Fig. 1. In order to achieve this result, we will perturb an unstable plane wave, corresponding to the lower branch in Fig. 1, with a randomly varying noise. This will produce a filamented phase, made of coherent structures whose shape remains qualitatively unchanged, up to smaller scale fluctuations [28].

In order to achieve the non-quantum liquefaction we have included both a linear incoherent pumping mechanism and nonlinear three-body losses [29]. In other words, we have considered $\delta = \delta^R + \mathrm{i}\delta^I$ and we have introduced a linear gain term $\mathrm{i}\Gamma\Psi$ in Eq. (1). This corresponds to a continuous load of particles in the system. Note that in this way, we are describing a more realistic non-conservative version of Eq. (1), which models an experimentally achievable scenario in the framework of current BEC experiments. In fact, in condensed matter systems it is possible to control the load of particles and two-body and three-body recombination within the coherent atomic cloud.

On the other hand, in nonlinear optics, such nonlinear models are well-known in the framework of complex Ginzburg–Landau (G–L) equations used to describe wide-aperture laser cavities [30]. Although it is always possible to control the linear gain introduced in the system, three-body losses are often imposed by the nonlinear response of the material, so it is not possible to manage the dissipative terms of the system. However, by means of electromagnetic induced transparency techniques, it is possible to customize the nonlinear optical response of cold atomic ensembles like Rb [11] so that the nonlinear refractive index corresponds to the one given by the modified Eq. (1) analyzed in the current section of the paper. Therefore our model, and its predicted

Fig. 3. [Color online] Numerical simulation of the evolution of a set of filaments in the presence of linear gain and three-body losses. Propagation algorithm parameters: $\gamma = 1$, $\Gamma = 10^{-2}$, $\delta = 1 + 0.1\mathrm{i}$. Top: pseudocolor maps of the amplitude. Bottom: pseudocolor maps of the phase corresponding to the amplitudes above. As can be appreciated in the sequence of snapshots, the initial condition, which has a certain level of organization, evolves towards a completely disordered situation, i.e., the diluted disordered gaseous phase arises. The horizontal (vertical) axis displays the spatial variable x (y) which is defined within the interval x (y) $\in [-175, 175]$ The frames correspond to values of the adimensional variable η: 0 ((a), (d)), 1000 ((b), (e)) and 4000 ((c), (f)).

phenomenon of liquefaction that we will demonstrate below, can correspond both to realistic BEC and to nonlinear optical systems.

In Fig. 3, the initial state consists of an incoherent set of filaments with a randomly varying phase distribution. Within this apparent disorder, some coherent uncorrelated structures (filaments) exist and can be observed in Fig. 3 (a). In this simulation, we have considered a nonlinear parameter regime where the linear gain was not enough to compensate for the three-body dissipative term. As a consequence, a certain degree of coherence is lost since the filaments disappear and only the noisy background is observed, as shown by snapshot (c) in Fig. 3.

Starting from the same initial condition but increasing the linear gain term over a certain threshold, we have performed the simulation shown in Fig. 4. In this case, we see that the system evolves towards a homogeneous plane wave because of the combined effect of adding particles to the initial random state and dissipation due to many-body inelastic processes. This relaxation process is well-known in the context of the complex G–L equations and is attributed to the non-conservative nature of the model [31]. The density of the resulting plane wave is set by the ratio between gain and loss

$$|\Psi|^2 \approx \sqrt{\frac{\Gamma}{\delta^l}}. \tag{6}$$

Obviously, for reaching a stable plane wave after the liquefaction process, the resulting density $|\Psi|^2$ must belong to the upper plane wave branch shown in Fig. 1. As can be appreciated in Fig. 3, the parameters used in the simulation give rise to a uniform density $|\Psi|^2 \approx \sqrt{0.1} \approx 0.3162$, which falls on the unstable plane wave branch. In contrast, in the simulation displayed in Fig. 4, we have chosen the parameters following this expression $\Gamma = (9/16)\delta^l$, so that in such a case, the spatially uniform solution obtained after numerical integration of the modified Eq. (1) has a density $|\Psi|^2 \approx \frac{3}{4}$, which corresponds to the plane wave of the stable "liquid" upper branch with an amplitude corresponding to the state of zero value of the grand potential density. Notice that this choice has been made in order to correlate the analytical results summarized in Section 3 for the conservative system governed by Eq. (1) and the numerical simulations of the non-conservative model discussed in the current section.

Very remarkably, during the process, vortex–antivortex pairs with topological charges $m_v = 1, m_{av} = -1$ are formed (see the bottom phase maps in Fig. 4), so the constant phase of the emerging coherent wave remains hidden by the overlapping of the different vortex rotating phase distributions. Vortices are very robust topological structures [12] and in our simulations they remain stable as far as we could follow the numerical simulations.

We must also stress that our simulations in Figs. 3–5 only display a square central region of an extensive light condensate of finite size which grows as the number of particles increases (see Fig. 6), due to the net gain of the system. Therefore, the combined effect of the real and imaginary parts of the nonlinear interactions is to increase the size of the beam, keeping the peak density constant.

Finally, we have considered the effect of replacing the linear gain term by a nonlinear gain term of the form $\mathrm{i}\chi|\Psi|^2$. In this situation, the numerical results are similar to those in Fig. 4, although it can be observed that in the last stage of the evolution the vortices are annihilated. We want to emphasize that this fact does not reveal an exclusive feature of the system with nonlinear gain, since we have performed such a simulation with a linear gain term $\Gamma = \chi$, where χ is the nonlinear gain coefficient considered in the simulation displayed in Fig. 5, and the vortex annihilation process was also observed. Anyway, we have seen a significant difference in the timescale of the process, i.e., for $\Gamma = \chi$, by considering that the nonlinear pumping mechanism vortices have disappeared faster than in the case of linear pumping,